Cancer Science

WILEY

Cancer Science

ORIGINAL ARTICLE OPEN ACCESS

Heterogeneity in Osteosarcoma Revealed by scRNA Sequencing: CLU+ Endothelial Cells as Key Players in Tumor Progression

Zhehao Dai[1] | Peng Xie[1,2] | Xiangzhi Bai[3,4,5] | Tang Liu[6] | Xiaoning Guo[6] | Lei Kuang[1] | Ping Mu[7,8] | Fangjin Lu[9,10]

[1]Department of Spine Surgery, The Second Xiangya Hospital, Central South University, Changsha, China | [2]Hunan Key Laboratory of Molecular Radiation Oncology, Xiangya Hospital, Central South University, Changsha, China | [3]Image Processing Center, Beihang University, Beijing, China | [4]State Key Laboratory of Virtual Reality Technology and Systems, Beihang University, Beijing, China | [5]Advanced Innovation Center for Biomedical Engineering, Beihang University, Beijing, China | [6]Department of Orthopedics, the Second Xiangya Hospital, Central South University, Changsha, China | [7]Department of Physiology, Shenyang Medical College, Shenyang, China | [8]Key Laboratory of Human Ethnic Specificity and Phenomics of Critical Illness in Liaoning Province, Shenyang Medical College, Shenyang, China | [9]Department of Pharmaceutical Analysis, Shenyang Medical College, Shenyang, China | [10]Shenyang Key Laboratory for Screening Biomarkers of Tumor Progression and Targeted Therapy of Tumors, Shenyang Medical College, Shenyang, China

Correspondence: Ping Mu (pingmu@symc.edu.cn) | Fangjin Lu (lufangjin@symc.edu.cn)

Received: 14 February 2025 | **Revised:** 18 June 2025 | **Accepted:** 29 June 2025

Funding: This work was supported by the Foundation of Spring Sunshine Program-Cooperative Research Project of the Ministry of Education, 202200846; Graduate Education and Teaching Reform Project of Central South University, 2024JGB087; Innovation and entrepreneurship education teaching reform research project of Central South University, 2022CG035; Hunan Provincial Health Commission Research Project, C202304077236; Natural Science Foundation of Hunan Province, 2024JJ5482; National Natural Science Foundation of China, 82373108.

Keywords: CLU+ endothelial cells | intratumoral heterogeneity | multi-region sequencing | osteosarcoma | single-cell RNA sequencing

ABSTRACT

Osteosarcoma is a common malignant bone tumor in children and adolescents, characterized by high heterogeneity and poor prognosis. The role of intratumoral heterogeneity (ITH) in osteosarcoma progression remains poorly understood. To explore this, we collected paired tumor tissue samples from the central region (CR) and peripheral region (PR) of six osteosarcoma patients and performed single-cell RNA sequencing. Our findings reveal significant microenvironmental differences between these regions. The CR harbors a higher proportion of tumor cells, while the PR contains a higher proportion of endothelial cells, particularly the CLU+ subcluster. Functionally, the CR hosts a higher proportion of immune-activated myeloid cells and tumor-infiltrating lymphocytes (TILs), whereas the tumor cells in the PR show increased activation of hypoxia-related pathways. In the PR, CLU+ endothelial cells (CLU+_ECs) promote tumor metastasis by interacting with tumor cells through various ligands, including collagen family members, via ITGB1. Furthermore, CLU+_ECs induce CD8+ T cell exhaustion via the Nectin2-TIGIT pathway, suppressing the anti-tumor immune response. Overall, our study highlights the substantial spatial heterogeneity in osteosarcoma and identifies CLU+_ECs in the peripheral region as promising therapeutic targets.

Abbreviations: CAFs, cancer-associated fibroblasts; CLU+_ECs, CLU+ endothelial cells; CR, central region; M1, macrophage type 1; M2, macrophage type 2; MAP, methotrexate, adriamycin, and cisplatin; MSCs, mesenchymal stem cells; OCs, osteoclasts; OS, osteosarcoma; PR, peripheral region; scRNA-seq, single-cell RNA sequencing; Th, T-helper cells; TILs, tumor-infiltrating lymphocytes; Treg, regulatory T cells.

Peng Xie and Zhehao Dai contributed equally to this work.

1 | Introduction

Osteosarcoma (OS) is the most common primary malignant bone tumor, primarily affecting children and young adults aged 12 to 18. It typically occurs in the metaphysis of long bones, such as the distal femur and proximal tibia [1, 2]. The introduction of high-dose combination chemotherapy in the 1970s significantly advanced osteosarcoma treatment and increased the 5-year survival rate to approximately 60%–70%. However, some patients continue to experience recurrence or metastasis, which results in a poor prognosis [3, 4].

The genetic instability of osteosarcoma, often characterized by high heterogeneity, presents a significant challenge to effective treatments [5, 6]. Osteosarcoma typically develops insidiously, with tumors often exceeding 5 cm in size by the time of diagnosis [7]. This growth pattern results in the establishment of multiple tumor subpopulations and non-tumor cell populations within the spatial cellular architecture. Furthermore, the administration of neoadjuvant chemotherapy and the uneven distribution of nutrients and oxygen across tumor regions further exacerbate tumor heterogeneity [8–10].

With the advent of single-cell RNA sequencing (scRNA-seq), a powerful method for unraveling ITH at single-cell resolution, a series of studies have explored the landscape of osteosarcoma using this advanced technology. These investigations have revealed robust resistant clone subpopulations and a spectrum of resistance mechanisms within osteosarcoma. Moreover, they have elucidated the dynamics of the transition from drug-resistant clone subpopulations to metastatic clone subpopulations [11, 12]. Malignant subpopulations within tumors have been identified as direct contributors to T-cell exhaustion, thereby facilitating immune suppression. Furthermore, scRNA-seq has elucidated the critical roles of diverse non-tumor cell subpopulations in the tumor microenvironment (TME) during osteosarcoma metastasis. Specific subgroups of cancer-associated fibroblasts (CAFs) have been recognized as active participants, directly interacting with malignant cells and driving the metastatic cascade. Concurrently, subpopulations of macrophages and CAFs indirectly promote tumor metastasis by enhancing angiogenesis [13, 14]. In contrast, within the tumor thrombus, a significant increase in M1-type macrophages, activation of the IFNγ pathway, and noticeable tumor immune activation suggest substantial disparities in cellular interactions across distinct regions and tumor microenvironments [15]. However, these studies examined tissues from only a single region within the tumor, which do not adequately capture the tumor's heterogeneity.

In tumors, particularly those with larger volumes, significant differences exist in both the tumor cells and microenvironment between the CR and PR of the same tumor. For instance, previous studies preliminarily identified regional heterogeneity in osteosarcoma through whole-exome sequencing (WES) during tumor evolution [16]. Moreover, studies have demonstrated that scRNA-seq can uncover significant genetic variations and microenvironmental differences across multiple tumor regions in various cancer types, including kidney cancer, glioma, and liver cancer [17–19]. Therefore, it is crucial to conduct a comprehensive investigation of osteosarcoma's spatial heterogeneity, encompassing disparities in the spatial distribution of tumor cells, immune cells, and stromal cells, as well as variations in their interactions across distinct regions of the TME at the single-cell level, in order to advance our understanding of the heterogeneity of osteosarcoma.

In this study, we collected tumor samples from six osteosarcoma patients and performed scRNA-seq analysis. We validated differences in microenvironment components and cell functions between the CR and PR of the tumor after chemotherapy. Notably, the PR exhibited a more pronounced hypoxic and immunosuppressive microenvironment. We also identified a distinct vascular subtype that plays a key role in both tumor metastasis and immune suppression, exhibiting a unique spatial distribution. This comprehensive approach has not only uncovered the intricate microenvironmental characteristics of osteosarcoma but also highlighted novel potential therapeutic targets.

2 | Material and Methods

2.1 | Human Patient Samples Collection

This study involved the collection of tumor samples from the central and peripheral regions of six osteosarcoma patients after chemotherapy at the Second Xiangya Hospital between 2021 and 2023 for scRNA-seq analysis. In addition, paraffin-embedded samples from 32 osteosarcoma patients, collected from 2013 to 2023, were utilized for IHC and mIHC validation. All patients had been diagnosed with osteosarcoma (OS) and underwent standard neoadjuvant chemotherapy, which included doxorubicin, high-dose methotrexate, cisplatin, and ifosfamide, prior to surgical intervention, from which tumor samples were obtained. The clinical characteristics of the patients included in this study are summarized in Table S1.

2.2 | Tissue Dissociation and Preparation

The fresh tissues were preserved in sCelLive Tissue Preservation Solution (Singleron) on ice within 30 min following surgery. The samples were washed three times with Hanks Balanced Salt Solution (HBSS), minced into small pieces, and then subjected to digestion with 3 mL of sCelLive Tissue Dissociation Solution (Singleron) using the Singleron PythoN Tissue Dissociation System at 37°C for 15 min. The resulting cell suspension was filtered through a 40-μm sterile strainer. Next, GEXSCOPE red blood cell lysis buffer (RCLB, Singleron) was added, and the mixture (cell: RCLB = 1:2, volume ratio) was incubated at room temperature for 5 to 8 min to eliminate red blood cells. Following centrifugation at 300 *g* for 5 min at 4°C to remove the supernatant, the pellet was gently resuspended in PBS. Finally, Trypan Blue staining was performed, and cell viability was evaluated using microscopy.

2.3 | RT and Amplification and Library Construction

Single-cell suspensions (2×10^5 cells/mL) in PBS (HyClone) were loaded onto a microwell chip using the Singleron Matrix Single

Cell Processing System. Barcoding beads were then collected from the microwell chip, followed by reverse transcription of the mRNA captured by the beads to obtain cDNA, which was then amplified by PCR. The amplified cDNA was fragmented and ligated with sequencing adapters. The scRNA-seq libraries were constructed according to the protocol of the GEXSCOPE Single Cell RNA Library Kits (Singleron). Individual libraries were diluted to 4 nM, pooled, and sequenced on the Illumina NovaSeq 6000 platform with 150 bp paired-end reads.

2.4 | Primary Analysis of Raw Read Data (scRNA-Seq)

Raw reads were processed to generate gene expression profiles using CeleScope version 1.5.2, version 1.9.0, and version 1.10.0 (Singleron Biotechnologies) with default parameters. Briefly, barcodes and UMIs were extracted and corrected from the R1 reads. Adapter sequences and poly-A tails were trimmed from the R2 reads, and the trimmed R2 reads were aligned against the GRCh38 (hg38) transcriptome using STAR (version 2.6.1b). Uniquely mapped reads were then assigned to exons with FeatureCounts (version 2.0.1). Successfully assigned reads with the same cell barcode, UMI, and gene were grouped together to generate the gene expression matrix for further analysis.

2.5 | ScRNA-Seq Analysis

The output datasets were analyzed in R (version 4.0.5) using the Seurat package (version 4.0.0) [20]. To ensure data quality, cells with fewer than 300 expressed genes or with more than 10% mitochondrial genes relative to the total expressed genes were excluded. Doublets identified by DoubletFinder (version 2.0.4) were also removed [21]. To mitigate batch effects, we integrated the samples using the default parameters of the "FindIntegrationAnchors" and "IntegrateData" functions in Seurat. The expression matrix was normalized with the "NormalizeData" function. Highly variable genes (HVGs) were identified using the "FindVariableFeatures" function. Dimensionality reduction and clustering of the expression matrix were performed by scaling the data with "ScaleData" and analyzing it with "RunPCA". The first 25 principal components were clustered using "FindClusters," and the resulting clusters were visualized using two-dimensional Uniform Manifold Approximation and Projection (UMAP) or *t*-distributed stochastic neighbor embedding (*t*-SNE) techniques. Cell groups were classified based on differentially expressed genes (DEGs) and established cellular markers from the literature. A comprehensive list of these cellular biomarkers is provided in Table S2. Differential expression analysis of overrepresented genes within individual clusters, compared to other clusters, was conducted using the Wilcoxon Rank-Sum Test via the "FindMarkers" function in Seurat. To identify malignant cell populations, we employed the scCancer (version 2.0.1) R package [22], which integrates the inferCNV algorithm to infer large-scale chromosomal copy number variations (CNVs) from single-cell RNA sequencing (scRNA-seq) data. Subsequently, overrepresented Gene Ontology (GO) biological processes specific to each cluster were identified using the "compareCluster" function within the "clusterProfiler" R package (version 4.8.2) [23]. Finally, cell–cell interactions between populations were analyzed using the 'CellPhoneDB' package (version 4.0.0) [24].

2.6 | Survival Analysis

The Gene Expression Profiling Interactive Analysis (GEPIA) database (http://gepia.cancer-pku.cn) is an online platform that employs standardized processing techniques to analyze RNA sequencing expression data from the TCGA projects. Using GEPIA's 'Survival' module, we examined the relationship between CD36 expression and cancer prognosis [25].

2.7 | Immunohistochemistry (IHC) and Multiplex Immunohistochemistry (mIHC)

Commercially available primary antibodies against ACKR1 (ab137044, Abcam), HIF1A (ab92498, Abcam), NECTIN2 (ab233384, Abcam), TIGIT (ab243903, Abcam), CD31 (66065-2-Ig, PROTEINTECH), CD36 (18836-1-Ig, PROTEINTECH), ITGB1 (12594-1-Ig, PROTEINTECH) and pFAK (83933-1-RR, PROTEINTECH) were used for IHC and mIHC. Tumor samples were subjected to fixation in 4% paraformaldehyde for 48 h post-surgical resection, followed by embedding in paraffin and slicing into 4 μm-thick sections. All sections were deparaffinized, rehydrated, and washed thoroughly. The paraffin sections were then baked at 65°C for 2 h, dewaxed, and hydrated with xylene and gradient alcohol. Antigen retrieval was performed using EDTA buffer (pH 9.0) or sodium citrate buffer (pH 6.0). Preincubation with antibody diluent was followed by sequential incubation with primary and secondary antibodies according to the experimental protocol. Multi-IHC staining was conducted using an OPAL 6-PLEX MANUAL DETECTION kit (NEL811001KT, AKOYA BIOSCIENCES), following the manufacturer's instructions. After primary antibody incubation, the slides were incubated with secondary antibodies, and tyrosine signal amplification was carried out. Subsequently, sections underwent microwave heat repair followed by the next round of staining. Upon completion of all stainings, 4′,6-diamidino-2-phenylindole was used to stain the nuclei.

2.8 | Statistical Analysis

Statistical analyses were performed using GraphPad Prism 8.0 software. Differences between groups were assessed using Student's *t*-test, one-way analysis of variance (ANOVA), and the Wilcoxon Rank-Sum Test. A $p < 0.05$ was considered statistically significant.

3 | Results

3.1 | Single-Cell Expression Atlas and Cell Type Identification in CR and PR OS TME

After chemotherapy, OS specimens exhibit noticeable macroscopic differences. The CR of OS displays significant ossification and necrosis, indicating a favorable chemotherapy response. In contrast, the PR often shows tumor tissues with

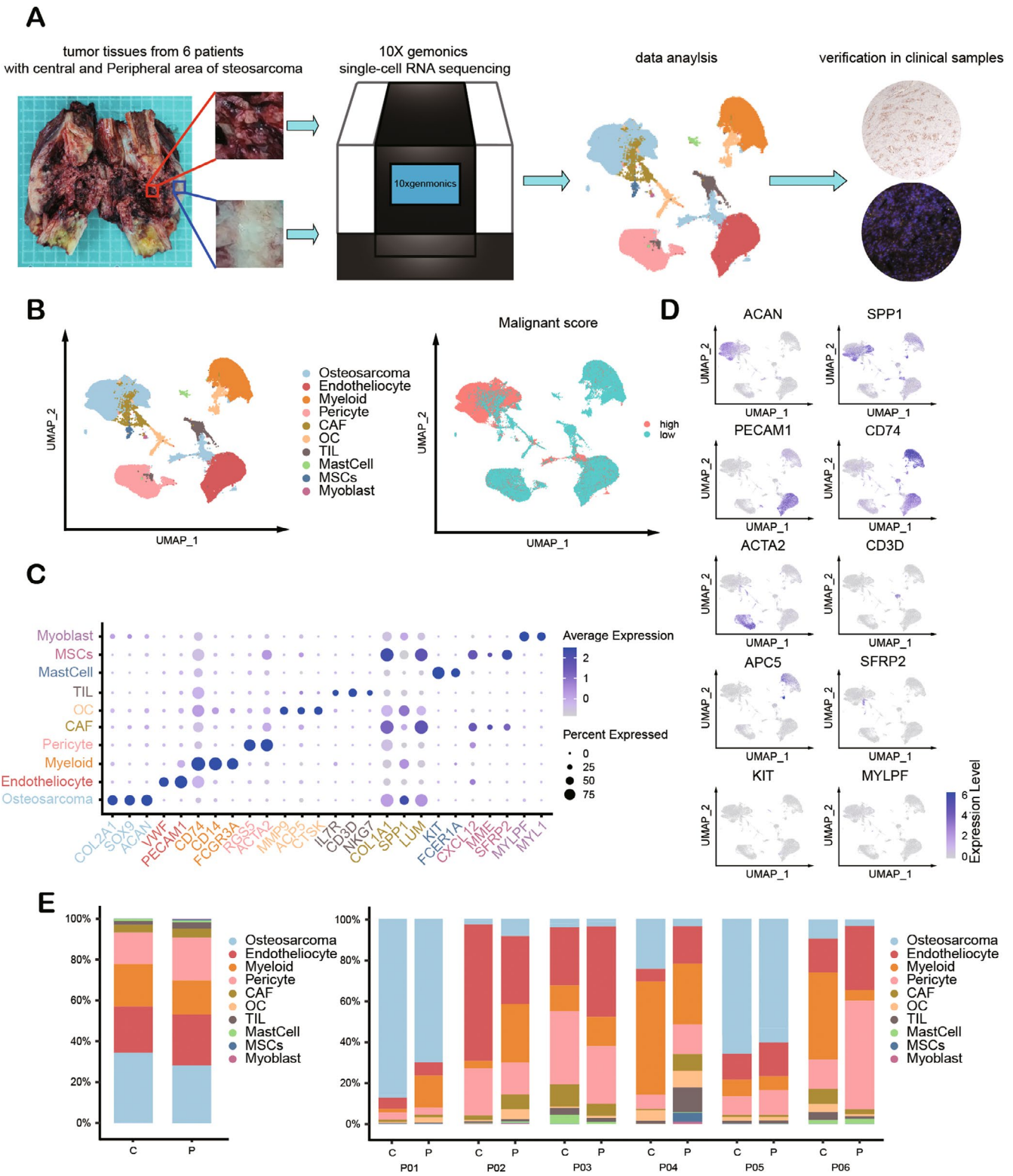

FIGURE 1 | Preliminary clustering of osteosarcoma single-cell sequencing. (A) Experimental flowchart. (B) Preliminary clustering UMAP plot and malignancy score plot. (C, D) Expression bubble plots and Umap plots of classic markers across the clusters. (E) Proportion plot of cells in CR (C, red) and PR (P, blue) (left), and distribution proportion of each cluster in individual patients (right).

a white or pale yellow, soft texture (Figure 1A). To comprehensively investigate the heterogeneity of OS, we performed scRNA-seq on paired CR and PR OS samples from six patients who underwent neoadjuvant chemotherapy with Methotrexate, Adriamycin, and Cisplatin (MAP) followed by surgical resection, and validated these findings through immunostaining (Figure 1A). After quality control and removal of batch effects between patients, we obtained 105,828 cells and identified 10 clusters using UMAP for dimensionality reduction and visualization (Figure 1B). Based on malignancy

score analysis, we labeled the clusters containing OS cells, while the remaining clusters were annotated using their canonical markers and gene expression features. Specifically, we identified myeloid cells (CD74, CD14), endothelial cells (PECAM1, VWF), pericytes (RGS5, ACTA2), cancer-associated fibroblasts (CAFs) (LUM, COL1A1), osteoclasts (OCs) (ACP5, MMP9), tumor-infiltrating lymphocytes (TILs) (CD3D, IL7R), mast cells (KIT, FCER1A), mesenchymal stem cells (MSCs) (SFRP2, CXCL12), and myoblasts (MYLPF, MYL1) (Figure 1C,D).

Through a comparative analysis of cellular proportions between the CR and PR, we observed an increased proportion of certain cell clusters, such as OS cells and myeloid cells, in the CR, while endothelial cells were more prevalent in the PR (Figure 1E). This variation was consistent across individual samples, suggesting a pronounced difference in the microenvironment composition between the CR and PR of OS.

3.2 | ITH Between CR and PR OS Cells

To investigate the heterogeneity of malignant cells between the two regions, we performed UMAP analysis of malignant OS cells, identifying 7 distinct malignant cell clusters (Figure 2A). The Chond_OS subcluster notably expresses higher levels of cartilage-related markers (SOX9, ACAN, COL2A1), while other subclusters show characteristics of osteogenic malignant cells, with higher expression of osteogenic markers (SPP1, COL1A1) (Figure S1A).

Notably, these subclusters exhibit significant spatial distribution differences. The Chond_OS cluster is more abundant in the CR, while the PR is enriched with the COL3A1+_OS cluster. GO enrichment analysis reveals that both the Chond_OS and COL3A1+_OS clusters are primarily associated with functions related to osteogenesis and vascular development regulation (Figure 2B, Figure S1B). These subclusters, representing chondrogenic and osteogenic malignant cells, are crucial to the malignancy of OS and are associated with circulatory metastasis. The IGKC+_OS subcluster, predominantly found in the PR (Figure 2B), exhibits elevated expression of immune globulin-related genes such as IGKC, IGHG1, and IGLC2, which are typically linked to enhanced tumor survival and metastatic potential, as well as immune suppression [26, 27].

Further GO analysis of malignant cell functions in the CR and PR of OS showed significant enrichment in osteogenesis and matrix formation in the CR, consistent with more pronounced osteogenic features in the tumor center (Figure 2C). In contrast, the Chond_OS and COL3A1+_OS clusters in the PR were enriched in functions related to hypoxia and aging (Figure 2C), suggesting the presence of a hypoxic microenvironment in the PR, which is associated with worse prognosis [28]. IHC analysis further confirmed that HIF1A expression exhibited significant differences between the CR and PR, with these differences observed exclusively in the metastatic group (Figure 2D,E). In conclusion, substantial differences in both the composition and functionality of malignant OS subpopulations were identified between the CR and PR.

3.3 | Characterization of Endothelial Cells in the CR and PR of Osteosarcoma

Hypoxia in the PR of the tumor often leads to increased proliferation of tumor-associated vessels. Except for patient #2, a higher proportion of endothelial cells was observed in the PR compared to the CR in all other patients (Figure 1E). Vessels in the PR exhibited more irregular morphology and increased density compared to those in the center (Figure S2A). To further investigate the differences in endothelial cells between the two regions, we performed UMAP clustering, identifying 9 distinct subsets from a total of 22,755 endothelial cells (Figure 3A).

Analysis of cell proportions revealed that while most cell subgroups were distributed relatively evenly, the CLU+_ECs cluster showed a pronounced distribution difference, being significantly more prevalent in the PR than in the CR (Figure 3B). This cluster exhibited high expression of MHC-II class molecule-related genes, suggesting their involvement in immune regulation, particularly in lymphocyte immunity and antigen presentation. GO enrichment analysis further confirmed that these cells are involved in the hypoxic response and epithelial cell migration (Figure S2B). This suggests that CLU+_ECs may be distributed in hypoxic environments, contributing to tumor immune regulation and metastasis. Additionally, immune regulation functions were enriched in the PR for CLU+_ECs (Figure S2C). ACKR1, a membrane protein highly expressed in CLU+_ECs, demonstrated greater specificity than other endothelial subclusters (Figure S2D). mIHC staining revealed significantly higher ACKR1 expression in vessels in the PR compared to the CR, with this difference particularly evident in metastatic patients (Figure 3C,D).

To evaluate the interaction between endothelial cells and malignant cells, we used CellPhoneDB. Our analysis showed that CLU+_ECs did not exhibit significant regional differences in regulating major malignant cell subgroups. However, distinct variations in how malignant cells regulate CLU+_ECs were observed. Specifically, tumor subgroups in the PR displayed significantly stronger regulation of CLU+_ECs while no significant difference in the VEGF pathway, which regulates vascular growth, was observed between the two regions. Tumor cells in the PR selectively activated specific interaction pathways with CLU+_ECs (e.g., matrix-related proteins like COL9A and COL6A-(ITGA2-ITGB1)), promoting tumor-associated vessel formation (Figure 3E). Consistently, mIHC confirmed a more pronounced activation of the ITGB1 pathway in the PR compared to the CR (Figure S3).

In summary, CLU+_ECs exhibits enhanced proliferation under the regulation of malignant cells in the PR, contributing to metastasis and immune modulation in OS.

3.4 | CLU+_ECs Suppress T-Cell Immunity in the Periphery of Osteosarcoma

To explore the impact of CLU+_ECs on OS immunity, we analyzed TILs, classifying them into seven distinct groups based

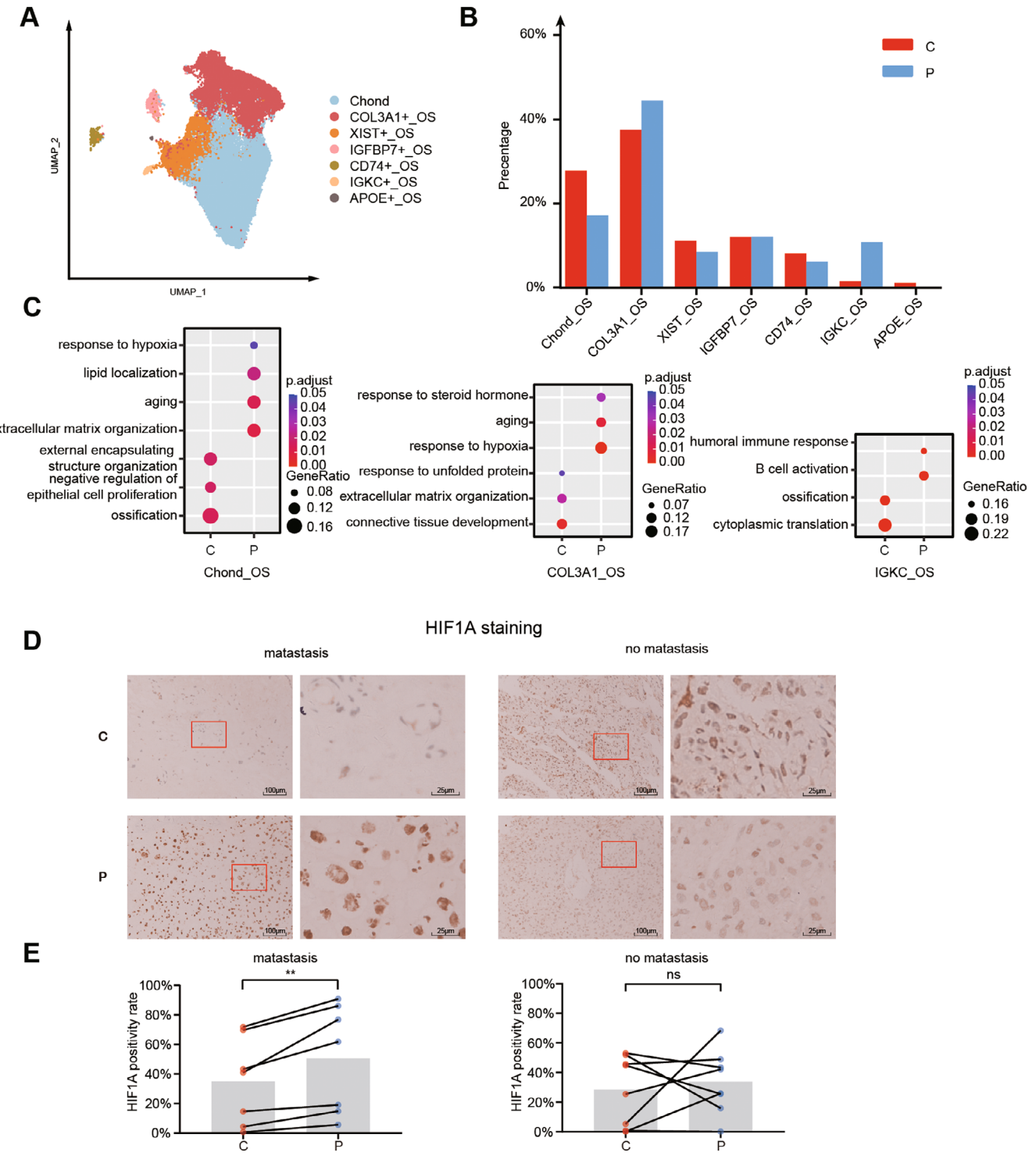

FIGURE 2 | Subcluster analysis of malignant cells. (A) UMAP plot of malignant cell subclusters. (B) Proportion differences of each subcluster between central and peripheral regions. (C) GO enrichment analysis comparing malignant subclusters in CR (C) and PR (P). (D) IHC images showing the expression of HIF1A in CR and PR of primary tumors from metastatic and non-metastatic patients. (E) Line bar graphs showing the differences in HIF1A positivity rates between CR and PR of tumors in metastatic and non-metastatic patients (**$p < 0.01$).

on molecular markers (Figure 4A). Two subsets of CD8+ Tc cells displayed elevated expression of cytotoxic genes such as GZMA and IFNG, while Treg cells showed increased expression of regulatory T cell markers like IL2RA and FOXP3 (Figure 4B). CD8+ Tc cells were more abundant in the CR compared to the PR (Figure 4C). CD8+ Tc1 cells in the PR exhibited increased expression of exhaustion-related genes (TIGIT, CTLA4) and were functionally enriched in negative immune regulation (Figure S4A, Figure 4D), indicating pronounced immune suppression in the PR TME. In contrast,

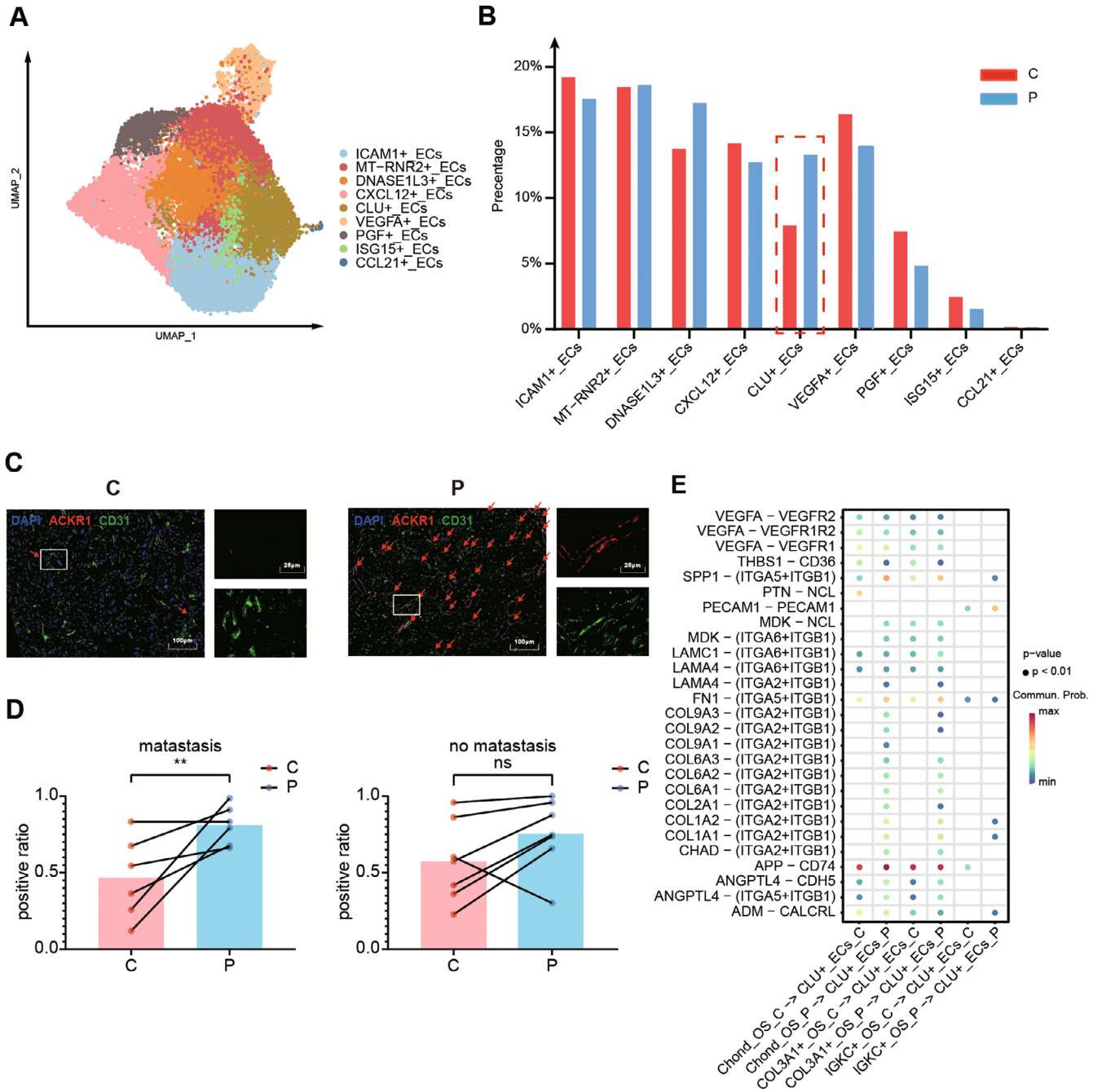

FIGURE 3 | Differential analysis of endothelial cells in CR and PR of osteosarcoma. (A) Umap plot displaying 10 subclusters of endothelial cell clusters. (B) Proportion plot showing the distribution differences of endothelial cell clusters between CR (C) and PR (P). (C) Multiplex immunofluorescence images showing ACKR1-positive vessels (red arrow) in CR (C) and PR (P). (D) Line bar graphs comparing the proportion of ACKR1-positive vessels in CR and PR, divided into metastatic and non-metastatic groups (**$p < 0.01$). (E) Cell interaction diagram between malignant cell subgroups and CLU+_ECs in CR (C) and PR (P).

CD8+ Tc1 cells in the CR were enriched in metal ion-related responses, likely due to higher chemotherapy drug concentrations (Figure 4D).

CellPhoneDB analysis revealed APP-CD74 interactions between TILs and CLU+_ECs in both regions, suggesting that CLU+_ECs may recruit immune cells through this pathway. In the PR, CLU+_ECs interact with Treg and Th cells via MHC-II, forming connections with CD4+ T cells, which may contribute to the dual recruitment of Treg and Th cells in the periphery. Notably, CLU+_ECs exclusively interact with NECTIN2-TIGIT and CD8+ Tc1, Treg, and Th cells in the PR (Figure S4B), a pathway associated with tumor immune suppression [29]. We propose that CLU+_ECs primarily suppress T-cell immunity at the tumor periphery.

To support this hypothesis, mIHC staining demonstrated that CLU+_ECs express NECTIN2 and are surrounded by TIGIT+ cells within a 50 μm radius, more prominently in tumors from patients with poor prognosis (Figure 4E,F). These findings suggest that the tumor periphery of OS is in an immunosuppressed state compared to the center, with CLU+_ECs playing a pivotal role in this process.

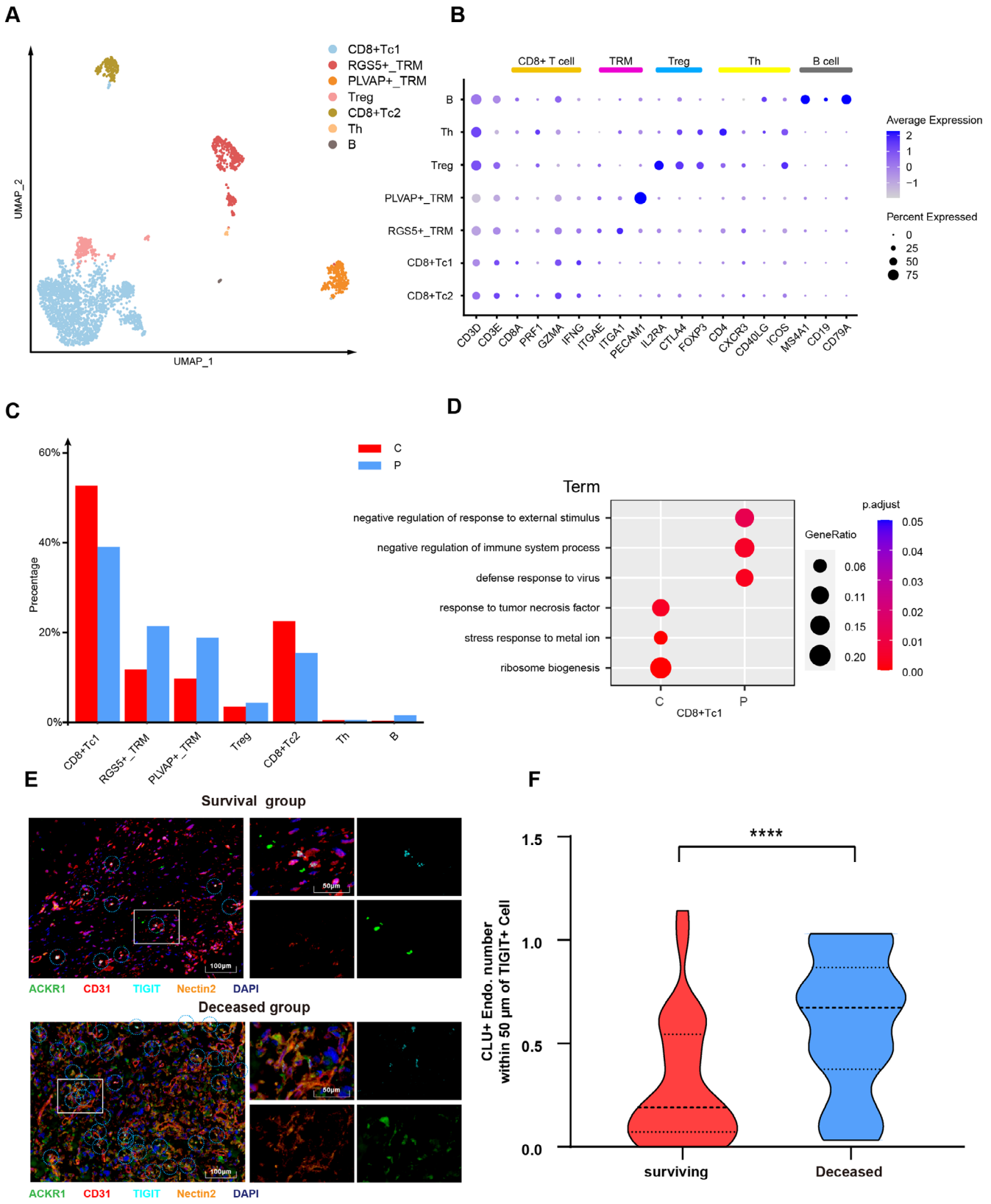

FIGURE 4 | Analysis of characteristics of TILs clusters in central and peripheral regions of osteosarcoma. (A) UMAP plot showing TILs divided into 7 subclusters. (B) Bubble plot displaying the expression of various classic markers across TIL subclusters. (C) Proportional distribution of TIL subclusters in the central and peripheral regions. (D) GO enrichment analysis revealing functional differences of CD8+ Tc1 between CR (C) and PR (P). (E) Multiplex immunofluorescence demonstrated the spatial relationship between the immune-exhausted phenotype TIGIT and CLU+ vessels (ACKR1+ and CD31+) in the survival and deceased groups. The blue dashed circles represent a 50 μm radius around the TIGIT+ cells. (F) Violin Plot Showing the Average Number of CLU+ Vessels Surrounding TIGIT+ Cells in Survival group and Deceased group.

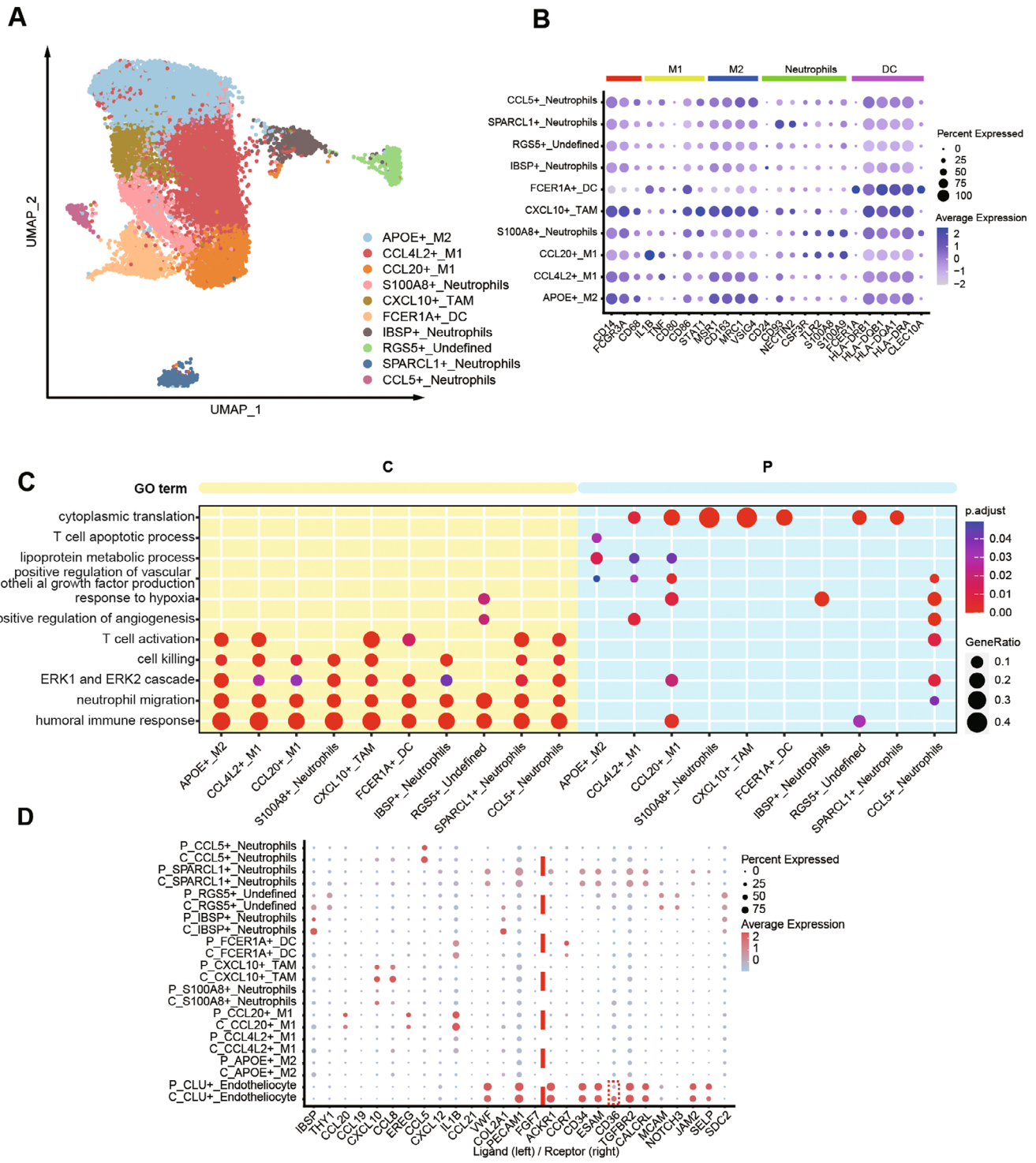

FIGURE 5 | Differential analysis of myeloid cells in central and peripheral regions. (A) Myeloid cells are divided into 10 subclusters on the UMAP plot. (B) Expression of molecular markers associated with various types of myeloid cells across the subclusters. (C) GO enrichment analysis based on differentially expressed genes between myeloid cell subclusters in the CR and PR. (D) Cell communication network between CLU+_ECs and myeloid cell subclusters.

3.5 | Myeloid Cells Contribute to an Anti-Tumor Immune Environment in the CR of Osteosarcoma

Myeloid cells, as key components of the tumor immune microenvironment, exhibit significant regional differences in their abundance between the CR and PR of osteosarcoma, underscoring the need for further exploration of their distinct biological roles. Our analysis identified 10 myeloid cell subgroups, including macrophages, dendritic cells, neutrophils, and others (Figure 5A). With the exception of APOE+_M2 and IBSP+_Neutrophils, the majority of myeloid cell subgroups did not show significant regional variations in their proportions (Figure 5B, Figure S5A). Specifically, APOE+_M2 cells were functionally

enriched in cholesterol metabolism and immune suppression (Figure S5A,B). The higher proportion of APOE+_M2 cells in the PR contributes to the establishment of an immunosuppressive environment in the PR. In contrast, IBSP+_Neutrophils were predominantly found in the CR, where they were functionally associated with tumor ossification and matrix formation (Figure S5A,B).

Notably, when comparing the functional enrichment of myeloid cell subgroups in the CR and PR, consistent changes in differentially expressed genes were observed. Myeloid subgroups in the CR showed upregulation of chemokine-related factors such as CCL2, CCL8, and CCL13, which were significantly enriched in immune response pathways, promoting the chemotaxis of neutrophils to the CR (Figure 5C). The enrichment of IBSP+_Neutrophils in the CR may be linked to this phenomenon. In contrast, myeloid cells in the tumor periphery did not exhibit the same enrichment pattern as those in the CR. Regarding cell interactions, no significant differences were observed in the receptors and ligands between myeloid cells in the CR and PR. However, the CD36 receptor on CLU+_ECs was significantly more expressed in the CR (Figure 5D, Figure S5C,D), primarily regulated by THBS1, expressed by myeloid subclusters such as IBSP+, CCL20+, and RGS5+. Moreover, CD36 expression was positively correlated with sarcoma survival (Figure S5E). This pathway inhibits tumor vascular formation, leading to fewer vessels associated with CLU+_ECs in the CR compared to the PR [30–32].

In summary, myeloid cell subgroups in the CR of osteosarcoma contribute to an immune-activating tumor microenvironment, which promotes tumor immunity and cytotoxic responses while inhibiting vascular formation.

4 | Discussion

Osteosarcoma is a heterogeneous tumor that contributes to poor prognosis and metastasis. Although spatial heterogeneity in osteosarcoma has been partially explored at the transcriptome level 16, validation at the single-cell level remains lacking, with single-cell sequencing providing a more detailed cellular analysis. Most current studies focus on a single tumor region [11–13, 15], missing spatial differences. To address this, we collected tumor samples from both the central (CR) and peripheral regions (PR) of six patients for single-cell sequencing. Our analysis revealed significant regional differences in cellular composition, phenotypes, and interactions, particularly the higher abundance of CLU+ tumor vascular subtypes in the PR, which may contribute to metastasis and immune suppression (Figure 6).

Further clustering identified nine malignant cell subtypes, with the chondrogenic subtype (chond group) more prevalent in the CR. These cells are resistant to chemotherapy and linked to poor prognosis [12]. The CR's richer blood supply may explain the higher proportion of chemotherapy-resistant cells. In response to chemotherapy, most tumor subtypes in the CR upregulated

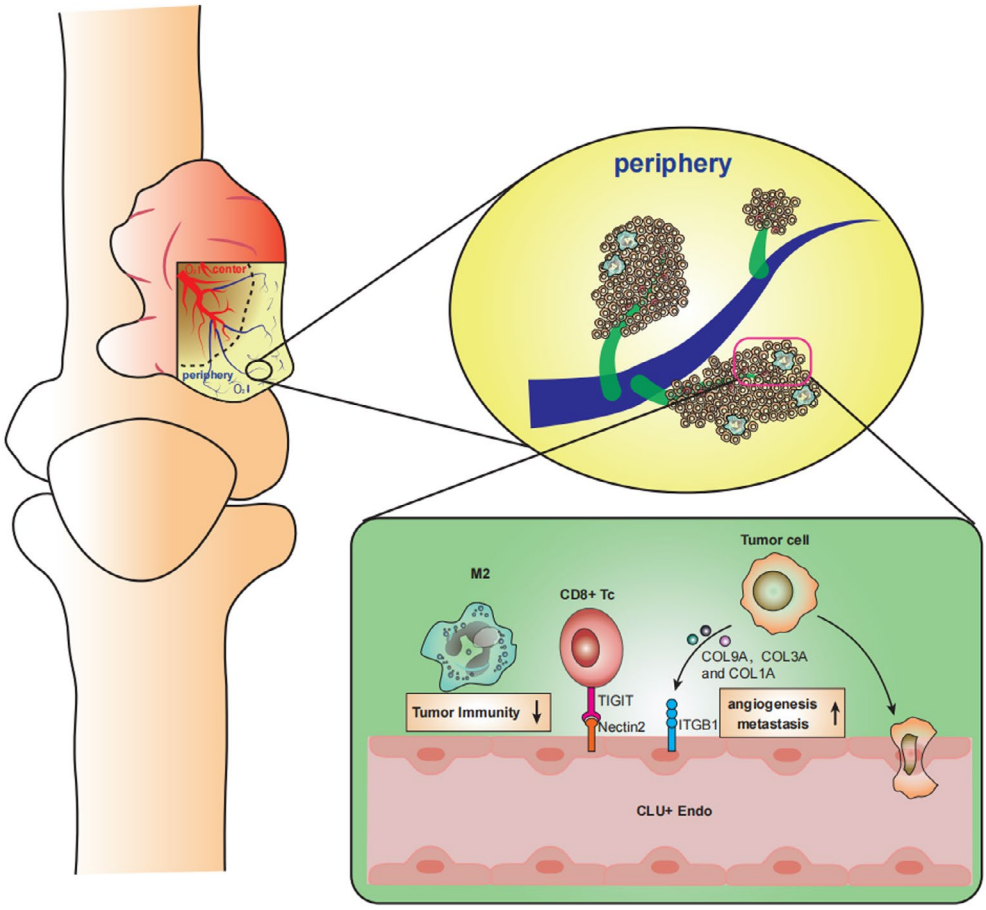

FIGURE 6 | Diagram of the peripheral tumor microenvironment in osteosarcoma.

osteogenesis and matrix-related genes, leading to ossification that hinders drug distribution and promotes hypoxia, which in turn enhances tumor growth and metastasis [33]. We confirmed this with high expression of hypoxia-related pathways in the malignant subtypes, and immunohistochemistry revealed higher HIF1A expression in the PR.

We also found a higher proportion of IGKC+_OS cells in the PR, which express immune evasion and metastasis-related genes [26, 27, 34]. However, no significant differences were found in bulk RNA sequencing related to prognosis, likely due to low cell representation. Further experiments are needed to elucidate their specific role in tumor biology.

Hypoxia is a well-known trigger for tumor angiogenesis [35], and studies have shown that CLU+ vasculature exhibits enhanced proliferative and migratory capacities [36]. CD31 staining revealed irregular blood vessels in the hypoxic PR, and clustering of endothelial cells showed a higher proportion of CLU+_ECs in the PR. While VEGFA-associated angiogenesis did not show spatial differences, other pathways, including ITGA and ITGB1 [37, 38], were more active in the PR, suggesting angiogenesis occurs independently of VEGFA. Additionally, CD36, typically anti-angiogenic [32], was expressed at lower levels in the PR, facilitating CLU+_EC proliferation. These cells also exhibited higher expression of MHC-II molecules and related immune functions, especially in the PR, suggesting a role in tumor immunity. While MHC-II is usually associated with immune activation [39, 40], our findings suggest that TILs in the PR express higher exhaustion markers (TIGIT) and have fewer CD8+ T cells, potentially interacting with CLU+ vessels via NECTIN2 and TIGIT to promote immune evasion. However, literature typically associates MHC-II expression with immune activation [41, 42], so further validation of this role in osteosarcoma is needed.

Despite being a "cold tumor" with limited lymphocyte infiltration after chemotherapy, osteosarcoma shows a higher proportion of myeloid cells, with more myeloid lineage cells in the CR. Further clustering revealed a predominance of M1-type macrophages and neutrophils in the CR, suggesting immune activation, while M2-type macrophages, which are immune-suppressive, predominated in the PR, pointing to an immune-suppressive environment in the PR. Similar patterns have been observed in lung cancer, with myeloid-derived macrophages showing spatial distribution differences. In osteosarcoma, hypoxia-driven accumulation of M2-type macrophages at the PR correlates with poor prognosis [43]. We also observed upregulation of chemotaxis-related genes (e.g., CCL2, CCL8, CCL13) in CR myeloid cells, which exhibited functions related to immune activation, neutrophil chemotaxis, and cytotoxicity. Similar differences between CR and PR in myeloid cells have been observed in breast cancer metastasis [44]. However, further studies are needed to clarify the role of these regional phenotypic differences in osteosarcoma progression.

In conclusion, our study demonstrates significant spatial differences in cellular composition and function between the central and peripheral regions of osteosarcoma. These differences include a hypoxic and immunosuppressive microenvironment in the PR, with potential implications for metastasis and treatment resistance. Our findings also suggest that CLU+_ECs may play a crucial role in osteosarcoma metastasis and immune evasion through ITGB1-related pathways and the Nectin2-TIGIT interaction, making it a potential target for osteosarcoma treatment.

Author Contributions

Zhehao Dai: conceptualization, data curation, funding acquisition, writing – review and editing. **Peng Xie:** data curation, validation, visualization, writing – original draft. **Xiangzhi Bai:** formal analysis, writing – review and editing. **Tang Liu:** resources, writing – review and editing. **Xiaoning Guo:** resources, writing – review and editing. **Lei Kuang:** resources, writing – review and editing. **Fangjin Lu:** conceptualization, formal analysis, funding acquisition, writing – review and editing. **Ping Mu:** project administration, resources, writing – review and editing.

Acknowledgments

We are deeply grateful to all the patients for their generous tissue donations. We also sincerely acknowledge Prof. Zhihong Li and his team for their valuable support in specimen collection, and Prof. Lunquan Sun and his team for providing laboratory facilities.

Ethics Statement

The primary osteosarcoma tissues were obtained from The Second Xiangya Hospital. All patients signed an informed consent to participate in the study before tissue donation. The study was reviewed and approved by the ethics committee of The Second Xiangya Hospital, Central South University (ethics number: 2023-LS-0264). This study was conducted in accordance with the principles of the Helsinki Declaration.

Conflicts of Interest

The authors declare no conflicts of interest.

References

1. F. Jafari, S. Javdansirat, S. Sanaie, et al., "Osteosarcoma: A Comprehensive Review of Management and Treatment Strategies," *Annals of Diagnostic Pathology* 49 (2020): 151654.

2. J. S. Whelan and L. E. Davis, "Osteosarcoma, Chondrosarcoma, and Chordoma," *Journal of Clinical Oncology* 36 (2018): 188–193.

3. S. Smeland, S. S. Bielack, J. Whelan, et al., "Survival and Prognosis With Osteosarcoma: Outcomes in More Than 2000 Patients in the EURAMOS-1 (European and American Osteosarcoma Study) Cohort," *European Journal of Cancer* 109 (2019): 36–50.

4. S. Ferrari, A. Briccoli, M. Mercuri, et al., "Postrelapse Survival in Osteosarcoma of the Extremities: Prognostic Factors for Long-Term Survival," *Journal of Clinical Oncology* 21 (2003): 710–715.

5. D. M. Gianferante, L. Mirabello, and S. A. Savage, "Germline and Somatic Genetics of Osteosarcoma - Connecting Aetiology, Biology and Therapy," *Nature Reviews. Endocrinology* 13 (2017): 480–491.

6. Y. Suehara, D. Alex, A. Bowman, et al., "Clinical Genomic Sequencing of Pediatric and Adult Osteosarcoma Reveals Distinct Molecular Subsets With Potentially Targetable Alterations," *Clinical Cancer Research* 25 (2019): 6346–6356.

7. S. S. Bielack, B. Kempf-Bielack, G. Delling, et al., "Prognostic Factors in High-Grade Osteosarcoma of the Extremities or Trunk: An Analysis of 1,702 Patients Treated on Neoadjuvant Cooperative Osteosarcoma Study Group Protocols," *Journal of Clinical Oncology* 20 (2002): 776–790.

8. V. Crenn, J. Amiaud, A. Gomez-Brouchet, et al., "Signature of the Vascular Tumor Microenvironment as a Marker of the Therapeutic Response to Doxorubicin in a Preclinical Model of Osteosarcoma," *American Journal of Cancer Research* 12 (2022): 1843–1854.

9. Y. Yuan, "Spatial Heterogeneity in the Tumor Microenvironment," *Cold Spring Harbor Perspectives in Medicine* 6 (2016): a026583.

10. A. Kashyap, M. A. Rapsomaniki, V. Barros, et al., "Quantification of Tumor Heterogeneity: From Data Acquisition to Metric Generation," *Trends in Biotechnology* 40 (2022): 647–676.

11. L. Wang, X. Huang, X. You, et al., "Nanoparticle Enhanced Combination Therapy for Stem-Like Progenitors Defined by Single-Cell Transcriptomics in Chemotherapy-Resistant Osteosarcoma," *Signal Transduction and Targeted Therapy* 5 (2020): 196.

12. Y. Zhou, D. Yang, Q. Yang, et al., "Single-Cell RNA Landscape of Intratumoral Heterogeneity and Immunosuppressive Microenvironment in Advanced Osteosarcoma," *Nature Communications* 11 (2020): 6322.

13. Y. Liu, W. Feng, Y. Dai, et al., "Single-Cell Transcriptomics Reveals the Complexity of the Tumor Microenvironment of Treatment-Naive Osteosarcoma," *Frontiers in Oncology* 11 (2021): 709210.

14. Y. Xu, C. Deng, H. Chen, et al., "Osteosarcoma Cells Secrete CXCL14 That Activates Integrin α11β1 on Fibroblasts to Form a Lung Metastatic Niche," *Cancer Research* 84 (2024): 994–1012.

15. T. Ji, Q. Shi, S. Mei, et al., "Integrated Analysis of Single-Cell and Bulk RNA Sequencing Data Reveals an Immunostimulatory Microenvironment in Tumor Thrombus of Osteosarcoma," *Oncogene* 12 (2023): 31.

16. D. Wang, X. Niu, Z. Wang, et al., "Multiregion Sequencing Reveals the Genetic Heterogeneity and Evolutionary History of Osteosarcoma and Matched Pulmonary Metastases," *Cancer Research* 79 (2019): 7–20.

17. C. Yang, S. Zhang, Z. Cheng, et al., "Multi-Region Sequencing With Spatial Information Enables Accurate Heterogeneity Estimation and Risk Stratification in Liver Cancer," *Genome Medicine* 14 (2022): 142.

18. Y. C. Shen, C. L. Hsu, Y. M. Jeng, et al., "Reliability of a Single-Region Sample to Evaluate Tumor Immune Microenvironment in Hepatocellular Carcinoma," *Journal of Hepatology* 72 (2020): 489–497.

19. R. Li, J. R. Ferdinand, K. W. Loudon, et al., "Mapping Single-Cell Transcriptomes in the Intra-Tumoral and Associated Territories of Kidney Cancer," *Cancer Cell* 40 (2022): 1583–1599.

20. A. Butler, P. Hoffman, P. Smibert, E. Papalexi, and R. Satija, "Integrating Single-Cell Transcriptomic Data Across Different Conditions, Technologies, and Species," *Nature Biotechnology* 36 (2018): 411–420.

21. C. S. McGinnis, L. M. Murrow, and Z. J. Gartner, "DoubletFinder: Doublet Detection in Single-Cell RNA Sequencing Data Using Artificial Nearest Neighbors," *Cell Systems* 8 (2019): 329–337.

22. W. Guo, D. Wang, S. Wang, Y. Shan, C. Liu, and J. Gu, "scCancer: A Package for Automated Processing of Single-Cell RNA-Seq Data in Cancer," *Briefings in Bioinformatics* 22 (2021): bbaa127.

23. G. Yu, L. G. Wang, Y. Han, and Q. Y. He, "clusterProfiler: An R Package for Comparing Biological Themes Among Gene Clusters," *OMICS* 16 (2012): 284–287.

24. M. Efremova, M. Vento-Tormo, S. A. Teichmann, and R. Vento-Tormo, "CellPhoneDB: Inferring Cell-Cell Communication From Combined Expression of Multi-Subunit Ligand-Receptor Complexes," *Nature Protocols* 15 (2020): 1484–1506.

25. T. Li, J. Fan, B. Wang, et al., "TIMER: A Web Server for Comprehensive Analysis of Tumor-Infiltrating Immune Cells," *Cancer Research* 77 (2017): e108–e110.

26. N. Niu, J. Zhang, T. Huang, et al., "IgG Expression in Human Colorectal Cancer and Its Relationship to Cancer Cell Behaviors," *PLoS One* 7 (2012): e47362.

27. X. Qiu, X. Zhu, L. Zhang, et al., "Human Epithelial Cancers Secrete Immunoglobulin g With Unidentified Specificity to Promote Growth and Survival of Tumor Cells," *Cancer Research* 63 (2003): 6488–6495.

28. Y. Lv, L. Wu, H. Jian, et al., "Identification and Characterization of Aging/Senescence-Induced Genes in Osteosarcoma and Predicting Clinical Prognosis," *Frontiers in Immunology* 13 (2022): 997765.

29. J. Wienke, L. L. Visser, W. M. Kholosy, et al., "Integrative Analysis of Neuroblastoma by Single-Cell RNA Sequencing Identifies the NECTIN2-TIGIT Axis as a Target for Immunotherapy," *Cancer Cell* 42 (2024): 283–300.

30. A. I. Sahora, A. W. Rusk, J. Henkin, E. M. McKeegan, Y. Shi, and C. Khanna, "Prospective Study of Thrombospondin-1 Mimetic Peptides, ABT-510 and ABT-898, in Dogs With Soft Tissue Sarcoma," *Journal of Veterinary Internal Medicine* 26 (2012): 1169–1176.

31. F. Haviv, M. F. Bradley, D. M. Kalvin, et al., "Thrombospondin-1 Mimetic Peptide Inhibitors of Angiogenesis and Tumor Growth: Design, Synthesis, and Optimization of Pharmacokinetics and Biological Activities," *Journal of Medicinal Chemistry* 48 (2005): 2838–2846.

32. D. W. Dawson, S. F. Pearce, R. Zhong, R. L. Silverstein, W. A. Frazier, and N. P. Bouck, "CD36 Mediates the In Vitro Inhibitory Effects of Thrombospondin-1 on Endothelial Cells," *Journal of Cell Biology* 138 (1997): 707–717.

33. T. Zhang, A. Kastrenopoulou, Q. Larrouture, N. A. Athanasou, and H. J. Knowles, "Angiopoietin-Like 4 Promotes Osteosarcoma Cell Proliferation and Migration and Stimulates Osteoclastogenesis," *BMC Cancer* 18 (2018): 536.

34. J. Tang, J. Zhang, Y. Liu, et al., "Lung Squamous Cell Carcinoma Cells Express Non-Canonically Glycosylated IgG That Activates Integrin-FAK Signaling," *Cancer Letters* 430 (2018): 148–159.

35. X. Jing, F. Yang, C. Shao, et al., "Role of Hypoxia in Cancer Therapy by Regulating the Tumor Microenvironment," *Molecular Cancer* 18 (2019): 157.

36. S. Hwang, D. H. Lee, I. K. Lee, Y. M. Park, and I. Jo, "Far-Infrared Radiation Inhibits Proliferation, Migration, and Angiogenesis of Human Umbilical Vein Endothelial Cells by Suppressing Secretory Clusterin Levels," *Cancer Letters* 346, no. 1 (2014): 74–83.

37. C. Su, J. Mo, S. Dong, Z. Liao, B. Zhang, and P. Zhu, "Integrinβ-1 in Disorders and Cancers: Molecular Mechanisms and Therapeutic Targets," *Cell Communication and Signaling: CCS* 22 (2024): 71.

38. J. Lee, J. Lee, W. Sim, and J. H. Kim, "Soluble TGFBI Aggravates the Malignancy of Cholangiocarcinoma Through Activation of the ITGB1 Dependent PPARγ Signalling Pathway," *Cellular Oncology* 45 (2022): 275–291.

39. K. Taguchi, T. Onoe, T. Yoshida, Y. Yamashita, Y. Tanaka, and H. Ohdan, "Tumor Endothelial Cell-Mediated Antigen-Specific T-Cell Suppression via the PD-1/PD-L1 Pathway," *Molecular Cancer Research* 18 (2020): 1427–1440.

40. A. O. Gkountidi, L. Garnier, J. Dubrot, et al., "MHC Class II Antigen Presentation by Lymphatic Endothelial Cells in Tumors Promotes Intratumoral Regulatory T Cell-Suppressive Functions," *Cancer Immunology Research* 9 (2021): 748–764.

41. A. C. Cunningham, J. G. Zhang, J. V. Moy, S. Ali, and J. A. Kirby, "A Comparison of the Antigen-Presenting Capabilities of Class II MHC-Expressing Human Lung Epithelial and Endothelial Cells," *Immunology* 91 (1997): 458–463.

42. J. Goveia, K. Rohlenova, F. Taverna, et al., "An Integrated Gene Expression Landscape Profiling Approach to Identify Lung Tumor Endothelial Cell Heterogeneity and Angiogenic Candidates," *Cancer Cell* 37 (2020): 21–36.

43. X. Zheng, A. Weigert, S. Reu, et al., "Spatial Density and Distribution of Tumor-Associated Macrophages Predict Survival in Non-Small Cell Lung Carcinoma," *Cancer Research* 80 (2020): 4414–4425.

44. I. Yofe, T. Shami, N. Cohen, et al., "Spatial and Temporal Mapping of Breast Cancer Lung Metastases Identify TREM2 Macrophages as Regulators of the Metastatic Boundary," *Cancer Discovery* 13 (2023): 2610–2631.

Supporting Information

Additional supporting information can be found online in the Supporting Information section.